Color-Based Sensing of Bending Deformation on Soft Robots

Rob B.N. Scharff, Rens M. Doornbusch, Xander L. Klootwijk, Ajinkya A. Doshi, Eugeni L. Doubrovski, Jun Wu, Jo M.P. Geraedts, and Charlie C.L. Wang*

***Abstract*— This paper introduces a novel approach for sensing the bending deformation on soft robots by leveraging multicolor 3D printing. The measurement of deformation enables to complete the feedback loop of deformation control on soft actuators. The working principle of our approach is based on using compact color sensors to detect deformation that is visualized by the change of color ratios. Two novel designs are presented to generate color signals on 3D printed objects, which we call an external signal generator and an internal signal generator. Signal processing and calibration methods are developed to transform the raw RGB-data into a meaningful deformation metric. Our experimental tests taken on soft pneumatic actuators verify that color signals can be stably generated and captured to indicate the bending deformation. The results also demonstrate the usability of this sensing approach in deformation control.**

I. Introduction

Sensors are widely used in robotic systems to provide feedback to achieve a precise control of operations. However, the compliance of soft actuators precludes the use of many conventional sensors such as encoders, metal / semiconductor strain gauges, or inertial measurement units for proprioception purposes [1]. As soft robots can deform in all directions throughout their entire body, sensors should be able to detect these unpredictable and large deformations. Moreover, ideal sensors for soft robots shall be bendable and/or stretchable, and shall have little influence on the performance of actuators. No off-the-shelf sensor meets these requirements.

A. Overview

This work presents a novel color-based sensing approach to provide feedback for active position control of soft pneumatic actuators. In these actuators, pressurized air is used to inflate air chambers. The geometrical asymmetry in the design or constituent materials drives the shape to deform in a desired way [1]. For example, bending can be realized through pressurization of an air chamber with an extensible top layer and an inextensible bottom layer. The basic idea of our deformation sensing approach is to translate the elongations that occur in the extensible parts of soft actuators into a measurable change of color ratios captured by a color sensor. This is achieved through flexible multi-color structures that can be easily fabricated and integrated in or onto soft actuators through multi-color *Additive Manufacturing* (AM).

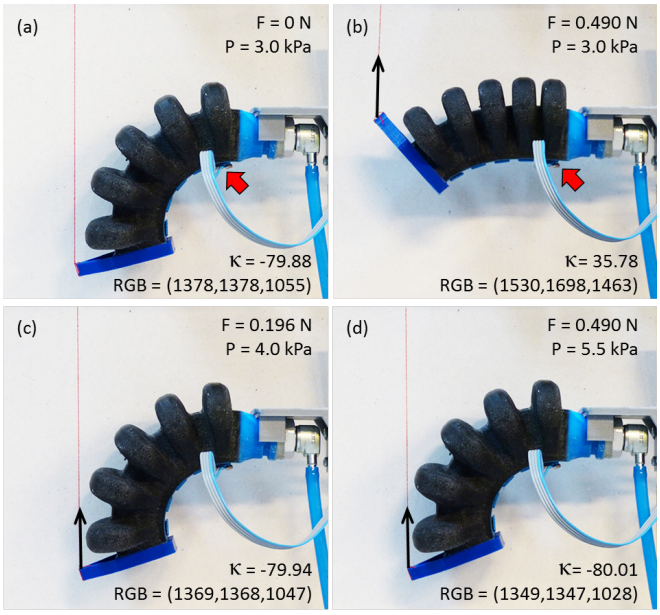

Fig. 1: An example to demonstrate the function of color signals for sensing deformations. (a) The deformation of a soft actuator under an air pressure of $3.0\,kPa$ serves as a reference. (b) The deformation is changed when an external force is applied to the tip of the soft actuator (indicated by the black arrow), under the same air pressure. The bending metric κ, calculated from the Red-Green-Blue (RGB) values measured by the color sensor, enables an accurate control of the deformation. Different external loads are applied in (c) and (d), the same deformation to (a) is achieved by increasing the air pressure until obtaining the same signal κ.

To interpret the raw RGB values obtained from the electric sensor and correlate them to the level of bending deformation, the signals are analyzed and transformed into a bending metric (κ). This metric can serve the purpose of controlling the deformation in a feedback control loop. Details of the signal analysis and calibration can be found in Section III.

For example, in the actuator shown in Fig.1, the RGB values are captured by an electronic color sensor placed near the root of the actuator (indicated by a red arrow in Fig.1(a) and (b)). It can be observed that, under a constant air pressure, the bending deformations without external force (a) and with an external force (b) are clearly different. Based on the difference in κ values, the air pressure is adjusted

All the authors are with the Department of Design Engineering, Delft University of Technology, 2628 CE, Delft, The Netherlands.

J.M.P. Geraedts and C.C.L. Wang are also associated with the TU Delft Robotics Institute.

*Corresponding Author: c.c.wang@tudelft.nl

until κ matches the value of κ for the reference bending (a). Fig.1(c) and (d) show that visually indistinguishable deformations corresponding to (a) can be achieved. Notice that different external forces are applied in (c) and (d), while they both have the same κ value. The experimental results of our sensing approach are further discussed in Section IV.

B. Related work

If the geometry of a task is known as a priori, the curvature of an actuator can be controlled through the applied pressure and mechanical programming (e.g., [2], [3]). For operations in complex and unstructured environments, mechanical programming becomes insufficient and sensors are needed.

Exteroceptive measurement of curvature can be achieved through a visual tracking system (e.g., [4]–[6]). However, proprioceptive sensing approaches have the potential to create more compact sensing systems and further improve the autonomy of soft robots. This requires sensors that can be integrated on soft actuators, such as draw wire encoders [7], resistive sensing using embedded conductive ink [8], [9], and highly flexible capacitive sensors built from conductive fabrics and silicone [10] or by depositing aluminum and silver layers on elastomer sheet [11], [12]. A more complete overview of sensing principles for soft actuators can be found in [13] and [14].

Attempts to further integrate sensors in soft actuators have been made through integration of resistive flex sensors or magnetic curvature sensors [15] in the inextensible layer during the fabrication process. Integration of sensors in other parts of the actuators requires the sensors to be stretchable as well. Zhao et al. demonstrate curvature control through integration of stretchable optical waveguides throughout an actuator in [16], [17]. Integration of eGain sensors in the dorsal surface of an actuator has been demonstrated in [18].

As the high flexibility of soft robots allows for many different deformations, most of the aforementioned work can use multiple sensors to measure the curvature more accurately or make a distinction between different types of deformation. As not all deformations are equally important, Wall et al. [19] developed a method to find an effective layout from a set of sensors. In this paper, we only study the functionality of a single sensor based on color signals.

C. Contribution

The technical contribution of our approach is twofold.

- A novel sensing principle integrating multicolored structures to serve as signal generators and thus provide feedback for deformation control.
- Signal processing and calibration methods for transforming raw color values into a meaningful bending metric.

Our sensing approach is contactless, easy-to-integrate, cost-effective and has a low power-consumption. As the measurements directly link to the geometry of the color printed 3D structures, our approach is less affected by external loading and time-related material response such as elastic hysteresis.

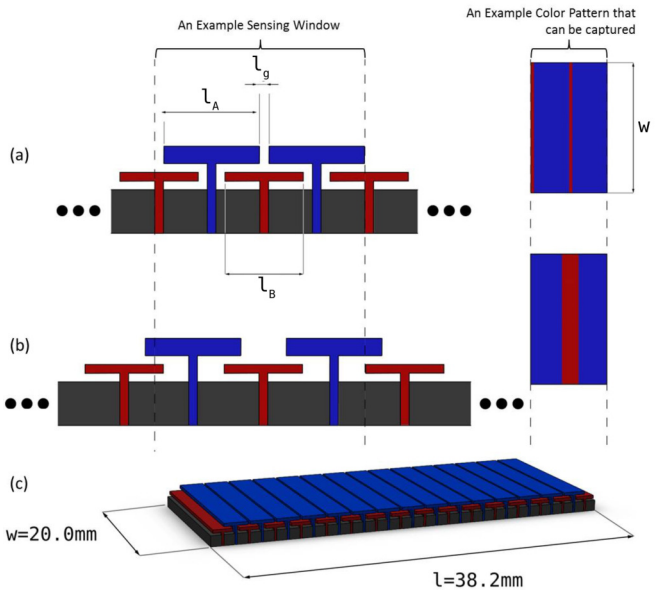

Fig. 2: Side view of the structure for an external signal generator in a released position (a) and a stretched position (b). The dimensions for T-components are $l_{\mathrm{A}} = 2.2\,\mathrm{mm}$, $l_{\mathrm{B}} = 1.8\,\mathrm{mm}$, and $l_{\mathrm{g}} = 0.2\,\mathrm{mm}$. Sixteen pairs of such T-components are periodically used in our design (c).

II. Signal Generator

Two embodiments of color-change generating structures are presented in this work: an external and an internal signal generators. We envision usage of the first embodiment in soft actuators where elongation of the air chamber is mainly based on material strain[1] (e.g. [20]), whereas the second embodiment is especially useful for actuators where elongation is mainly realized through bellow-like geometries (e.g. [21]). Note that we use two contrasting colors instead of black-and-white patterns to enable filtering out intensity fluctuations that occur due to the changing structure, as explained in Section III. The use of color also allows us to further extend the signal generators described below by embedding more colors in the structures, which generates more color patterns and therefore is able to sense more complicated deformations.

A. External signal generator

The first embodiment of our approach is a structure composed of T-shaped components with alternating height and color, embedded onto a highly stretchable and light-absorbing material (see Fig. 2). A color sensor captures signals from the top-view of the structure. When being stretched, the lower T-component become less occluded by the higher components – i.e., having more area observed through the sensing window so that the ratio of colors changes. The measurement of this color ratio is used to indicate the amount of strain.

[1]Although we test the external generator on a bellow-based pneumatic actuator.

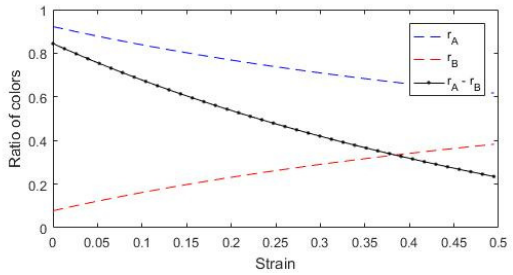

Fig. 3: The ratios of the exposed surface area of A and B components (i.e., $r_A(\epsilon)$ and $r_B(\epsilon)$) and their difference are all monotonic functions of the strain presented on the belt. The curves are generated by the structure shown in Fig.2.

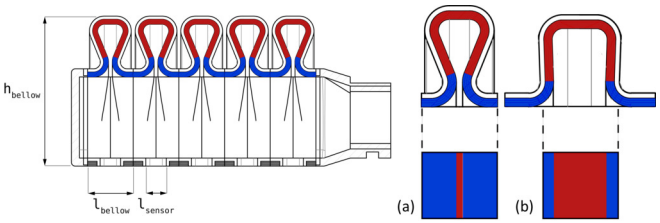

Fig. 4: An illustration of a bellow before (a) and after (b) being pressurized. The pattern of colors that can be captured through the sensing window is also shown at the bottom. (b) shows a larger red region can be 'seen' through the window in the presence of a large bending deformation. In this example, the dimensions of a bellow are $l_{\text{sensor}} = 5.1\,\text{mm}$, $l_{\text{bellow}} = 11.3\,\text{mm}$ and $h_{\text{bellow}} = 37.0\,\text{mm}$.

The structure is divided into a number of periods, with a period defined as the smallest repeating structure:

$$p = l_{\text{A}} + l_{\text{g}} + \Delta l. \tag{1}$$

Here l_{A} is the length of a high T-shaped component, l_{g} is the initial gap size, and Δl is the change in length of the non-occluded part of a low T-shaped component l_{B} upon stretching. Considering that the width w of a structured strip is constant, the ratio of areas exposed to the sensing window can be calculated by

$$r_{\text{A}} = \frac{l_{\text{A}}}{p}, \quad r_{\text{B}} = \frac{l_{\text{g}} + \Delta l}{p}, \tag{2}$$

for the ratio of the high T-shaped component A and low T-shaped component B respectively. Note that this is only valid when $\Delta l \leq l_{\text{B}} - l_{\text{g}}$; otherwise, the flexible base material will be exposed to influence the quality of color signal. Strain in the flexible base material can now be obtained as:

$$\epsilon = \Delta l/(l_{\text{A}} + l_{\text{g}}). \tag{3}$$

The relation between the color ratios and the strain are plotted in Fig.3 for the structure given in Fig.2. It can be found that the ratio difference $((r_{\text{A}}(\epsilon) - r_{\text{B}}(\epsilon)))$ is monotonic and also very sensitive to the strain presented on our color signal generator.

Note that the size of a sensing window is not taken into account here. Fluctuations of the signal presented in Fig.3 will be generated when a non-integer amount of periods is visible within the sensing window. This will be further discussed in Section III. As we aim to design a structure that can generate a consistent signal regardless of where the color sensor is placed, this error is minimized by minimizing the length of a period.

B. Internal signal generator

The second embodiment of our design is a color signal generator integrated into an existing design of a soft pneumatic actuator. This is realized by colorizing different regions of an Ω-shaped bellow in different colors, as illustrated in Fig.4. A color sensor is embedded in the inextensible layer of the bending actuator. Upon pressurization of the air chamber, the inflation of the bellows leads to a larger area of the originally occluded color being exposed to the window of the color sensor. As a result, the measurement of the sensor changes accordingly. The same sensing strategy can be applied to bellow-based pneumatic actuators of different shapes and dimensions. Although the measurements are strongly dependent on the particular design of an actuator, a general calibration procedure as discussed in the next section of this paper can be conducted to link the measurements of a color sensor to the level of bending deformation presented on the bellows.

C. Materials & Fabrication

The hardware realization of the color-change generating structures is shown in Fig.5.

The external signal generator is attached on top of an existing soft pneumatic actuator. One end of the belt is mounted at the root of the actuator, while the other end is attached to the tip of the bellow. The color sensor is also placed at the root of the actuator. When the actuator is bent, the structure elongates underneath the sensing window to generate color signals.

For the internal signal generator, miniaturized sensors were designed and mounted onto plugs. These plugs are inserted in the inextensible layer of the actuator. The number of sensors and the location of the sensors can be easily adjusted in our design. Our experimental results are obtained by a single sensor mounted at the root of the actuator. The outside of the plug and inside of the plug opening are built from rubber-like photopolymer (Agilus 30) that seals the air chamber. No air leakage was observed upon full actuation.

The embodiments of our design are fabricated on a Stratasys Objet 350 Connex3 Multi Material 3D printer, which uses Material Jetting technology and can print combinations of up to three different building materials together with a water soluble supporting material. All examples shown in our paper are printed using a combination of the flexible Agilus 30 Black, the rigid VeroCyan and the rigid VeroMagenta. Note that 3D printing materials with pure blue or red colors are not available.

The Agilus 30 Black has an elongation of $220 \sim 270\%$ at break and a tensile strength of $2.4 \sim 3.1\text{MPa}$ – as

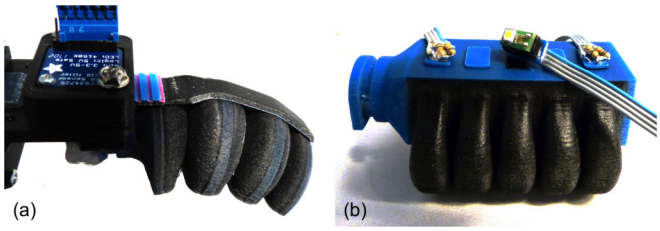

Fig. 5: Hardware realization of our color-based deformation sensing approach on 3D printed soft actuators in an external way (a) and an integrated manner (b). For illustrating the flexibility of our design, three sensors are presented in (b) although all the experimental results presented in this paper are obtained by placing a single sensor at the root of the actuator.

documented by Stratasys. The RGB values of the VeroCyan (VC) and VeroMagenta (VM) materials are $RGB_{\mathrm{VM}} = (166, 33, 98)$ and $RGB_{\mathrm{VC}} = (0, 93, 127)$ respectively. Brunton et al. [22] have characterized the VeroCyan and the VeroMagenta materials as highly translucent. We find that VeroMagenta has an even higher translucency than VeroCyan. Since translucency of the upper layer will decrease the color difference upon stretching, the VeroCyan material was chosen for the higher T-components in the external design and for the region near the 'neck' of air chambers in the integrated design.

III. Signal Analysis and Processing

This section starts with an analysis of the signals that are captured by our sensing approach, and then proceeds to a method for converting RGB values into a deformation metric κ. Remaining fluctuations in the signal is explained by simulations. After that, we introduce the calibration method.

A. Raw-data of color signal

A TCS34725 light-to-digital converter with an integrated white LED is used for the measurement of RGB colors. A miniaturized version of this sensor was designed to be mounted on the sensor plugs of the internal signal generator (see Fig.5(b)). For both embodiments, we use an integration time of $154\,\mathrm{ms}$ and 1X gain setting to obtain different RGB values from the converter when different color patterns are exposed to the sensing window. The TCS34725 sensor returns four values for each exposure, namely the R-, G-, B-components of color plus the light intensity.

To capture a set of raw data to conduct the signal analysis, we clamp a sample of our external signal generator onto a tensile testing machine. The sensor is then placed in a case having a window with dimensions $10\,\mathrm{mm} \times 12\,\mathrm{mm}$ (see Fig.6). The distance between the belt and the sensor is $4\,\mathrm{mm}$, and the sensing window is positioned at the boundary of the second period on the belt. A light absorbing cover is attached to the case of sensing to shield the belt from environmental light. Note that we use the same sensing window for the external sensing belt mounted on the bending actuator (see Fig.5(a)). The tensile testing machine moves the upper clamp upwards to stretch the belt in steps of $0.5\,\mathrm{mm}$ while the colors are measured for each step. The color sensor is connected to the lower clamp and remains fixed.

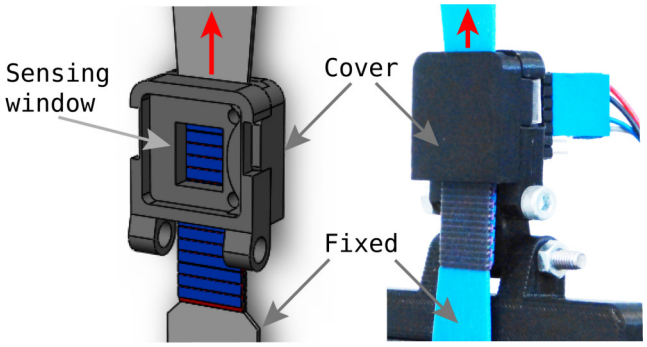

Fig. 6: The measurement setup for testing the sensor belts. The stretching direction is indicated with a red arrow.

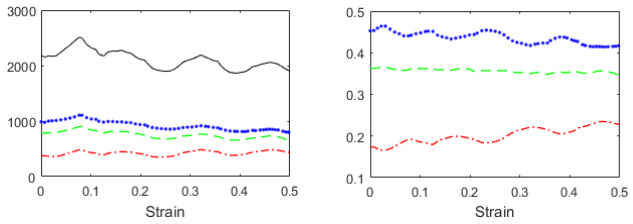

Fig. 7: (Left) The raw data of red (dash-dot), green (dashed), blue (dotted) and light-intensity (full line) obtained from a color-based sensing setup as shown in Fig.6. (Right) Normalized RGB by dividing by the measured light-intensity.

Figure 7 shows a typical RGB measurement of an external signal generator with a VeroCyan top and a VeroMagenta bottom layer in a tensile test with strain ranging from 0 to 0.5. Besides the change in colors, stretching the sensing belt also affects the measured overall intensity. Due to changes in reflectivity, shadows, distance-to-sensor and the underlaying materials, the intensities of the R-, G- and B-components go up or down simultaneously, which thereby distorts the signal. The same phenomenon is also observed for the integrated design. Normalizing the RGB-data by the intensity does not give a monotonic signal either. A more sophisticated method is presented in Section III-B.

B. Signal processing

As can be found in Fig.7, the RGB raw data shows a trend of increase in red and decrease in both blue and green. According to the RGB values of VeroMagenta (VM) and VeroCyan (VC) materials $RGB_{\mathrm{VM}} = (166, 33, 98)$ and $RGB_{\mathrm{VC}} = (0, 93, 127)$, it can be found that the change of colors in three components is indicating the increase of VeroMagenta and the decrease of VeroCyan. A naive processing of the RGB signals would therefore be

$$f = -I_{\mathrm{R}} + I_{\mathrm{G}} + I_{\mathrm{B}}, \tag{4}$$

which accumulates the trend of three components, I_{R}, I_{G} and I_{B}, into a single signal. Note that, if a positive weight

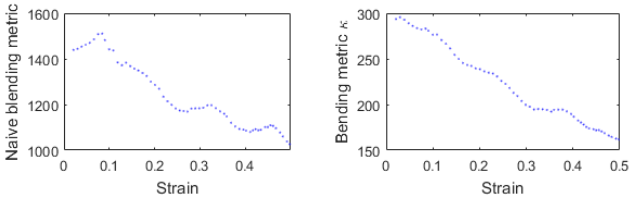

Fig. 8: Processing color signals into a metric of deformation – (left) by a naive blending scheme (as Eq.(4)) and (right) by a weighted blending scheme (as Eq.(5)).

is placed in front of I_{R}, the increasing of red will somewhat cancel out the decrease of I_{G} and I_{B} which leads to a less significant signal. A problem of processing by Eq.(4) is that it does not result in a monotonic function – i.e., fluctuations still exist (see the left of Fig. 8). We can eliminate the intensity peaks where R, G and B components move up in intensity with an equal amount (as shown on the left of Fig. 7), by adding weights to the intensities that sum up to zero. Our experimental tests show that using the normalized difference between VeroCyan and VeroMagenta as weights can generate a monotonic function $\kappa(\cdot)$. The weighted integration of I_{R}, I_{G} and I_{B} can be defined as

$$\kappa = (\hat{R}_{\mathrm{C}} - \hat{R}_{\mathrm{M}})I_{\mathrm{R}} + (\hat{G}_{\mathrm{C}} - \hat{G}_{\mathrm{M}})I_{\mathrm{G}} + (\hat{B}_{\mathrm{C}} - \hat{B}_{\mathrm{M}})I_{\mathrm{B}}, \quad (5)$$

where the normalized RGB components of VeroCyan and VeroMagenta are $(\hat{R}_{\mathrm{C}}, \hat{G}_{\mathrm{C}}, \hat{B}_{\mathrm{C}}) = (0, 0.4227, 0.5773)$ and $(\hat{R}_{\mathrm{M}}, \hat{G}_{\mathrm{M}}, \hat{B}_{\mathrm{M}}) = (0.5589, 0.1111, 0.3300)$.

For the internal signal generator, this results in a very sensitive monotonic signal as demonstrated in Section IV and the supplementary video. For the external generator, the signal is also monotonic, with some small fluctuations occurring at higher strains (see the right of Fig. 8). These fluctuations are an artifact of the sensing window, as will be discussed in Section III-C.

C. Simulation

From the normalized signal of colors shown on the right of Fig. 7, we can observe fluctuations where the intensities of red and blue move in opposite directions. These fluctuations occur whenever a non-integer amount of periods is visible within the sensing window. The color of the material moving in and out of the sensing window causes the variations of ratios r_A and r_B going up or down. About the influence of the sensing window on the fluctuations of color signals, the following observations are found:

- **Size of sensing window** – The fluctuations diminish with an increase of window size. Similarly, the same phenomenon can be found when decreasing the length of the T-components – this is equivalent to enlarging the relative size of a sensing window.
- **Position of sensing window** – The fluctuations appear at different regions of strains when we place the sensing window at different places. However, the appearance of fluctuations cannot be avoided at any place.

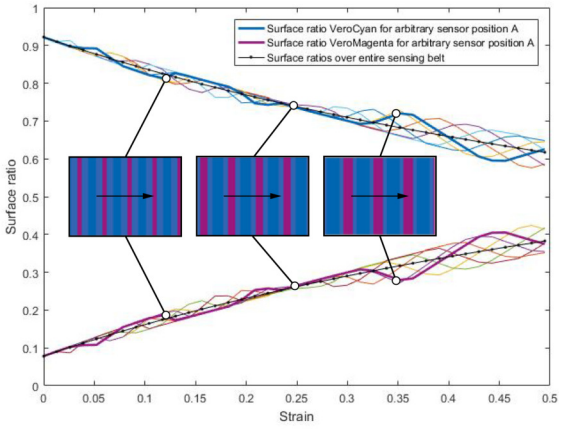

Fig. 9: Simulation of stretching tests – the signals are obtained by placing the sensing window at six different positions. The color patterns that can be observed through a sensor window are also displayed for a few different strains.

A simulation was conducted to study these influences as shown in Fig.9, where the sensing window is placed at the boundary of the second period of the sensing belt and shifted over the length of a period of the structure in six steps. At each place, our simulator generates a curve indicating the ratio of the cyan region's area over the window's area (the top curve) and a curve according to the ratio of the magenta region's area (the bottom curve). Moreover, we also generate two curves by (1) using the total area of all cyan regions over the area of the entire sensing belt and (2) using the total area of all magenta regions over the entire structured strip, which are displayed in black with dots. These two curves serve as ideal signals as they are not influenced by the above two factors – i.e., size and position of sensing window.

The simulation results shown are consistent with the results presented on the right of Fig.7 and Fig.8. When having a large deformation, the relative size of the sensing window as compared to the dimensions of the periods becomes small. As a result, larger fluctuations appear on the signals.

D. Calibration

With the help of the processed signals as shown in the right of Fig.8(b), we are able to determine an algebraic function $\epsilon(\kappa)$ indicating relationship between color-signal and the level of deformation by a calibration process. Specifically, the parameters of the following function are determined by a least-square fitting,

$$\epsilon(\kappa) = a + b\kappa + c\log(\kappa). \quad (6)$$

For the sensing belt data shown in the right of Fig.8, we obtain $a = 4.845$, $b = -0.0005137$ and $c = -0.8711$ with R-square being 0.9899.

Similar to stretching tests, bending tests are conducted on the integrated design. We calibrate a function $\alpha(\cdot)$ in terms of bending 'angle'. That is

$$\alpha(\kappa) = \tilde{a} + \tilde{b}(\kappa + \tilde{d}) + \tilde{c}\log(\kappa + \tilde{d}), \quad (7)$$

with α indicating the level of deformation (e.g., bending angle of the bellow that is captured by the sensor, as shown in Fig.12 C). As negative values are allowed for the bending metric κ, a coefficient $\tilde{d}$ is added to ensure the validity of a $\log(\cdot)$ function. The calibrated coefficients for the bellow shown in Fig.12 are $(\tilde{a}, \tilde{b}, \tilde{c}, \tilde{d}) = (2038, 0.1133, -303.3, 1301)$ with R-square being 0.9968. Each newly printed strip or bellow needs to be calibrated, as the performance is also dependent on the fabrication process.

IV. Experimental Results

This section discusses the experimental results of our sensing approach. Both actuator embodiments and the separate sensing belts have been tested under extreme lighting conditions, ranging from near darkness to illumination by two Menik LS-1200 LED panels (with $7380\,\mathrm{Lumen}$) placed at a distance of $20\,\mathrm{cm}$ on both sides of the actuators. The differences in bending metric caused by lighting variation were marginal, as is also demonstrated in the supplementary video material by turning off the LED panels during measurement.

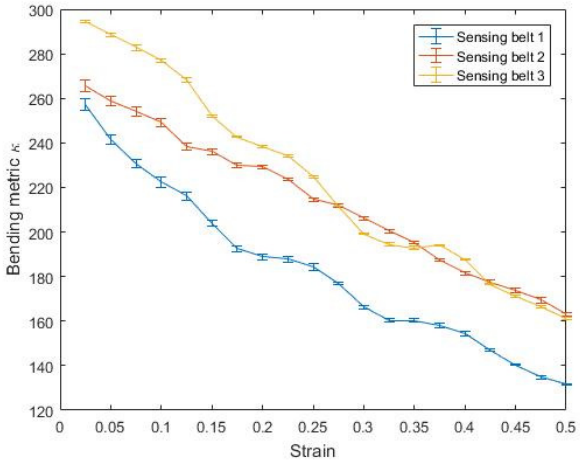

Fig. 10: Average result of the bending metric κ over five measurements for three different sensing belts. The standard deviations are indicated along with the curves.

A. Results by external signal generator

Three identical sensing belts have been 3D-printed and tested using the setup described in Section III. Each sample was tested five times using the same clamping. The raw data points were re-sampled at every step of 0.025 in the strain. An average was calculated for the five tests, and the standard deviations are shown as well in Fig.10. Although a separate calibration is needed for each sensing belt, different measurements of the same belt are very consistent. Integration of the sensing belt on a bending actuator to control the position and detect obstacles is demonstrated in Fig.11. Upon touching an object, the bending metric κ starts to deviate from the curve corresponding to collision-free motion.

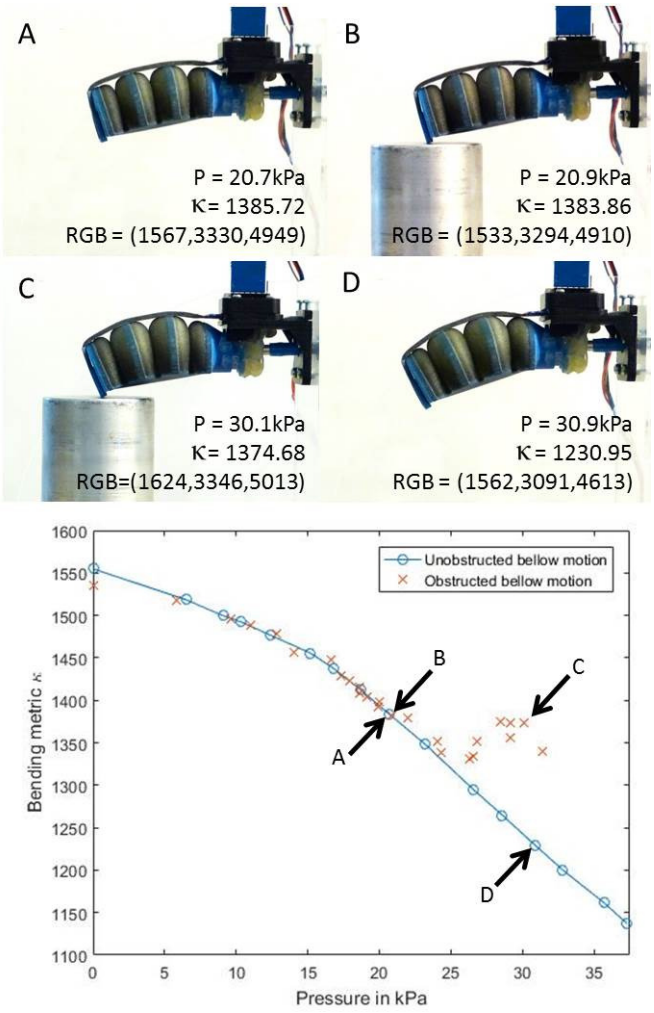

Fig. 11: Before and until the moment of touching, the measured bending metric κ of the bellow's motion follows that of the collision-free motion (A & B). Upon touching, the bending metric of an obstructed bellow (C) deviates from the unobstructed bellow (D) when the same pressure is applied.

B. Results by internal signal generator

A single miniaturized color sensor was used and placed at the first bellow of the integrated design (as indicated in Fig.1). The progressive results of the integrated sensing approach are shown in Fig.12. Here, the bending metric is plotted with reference to the pressure during unobstructed bending. Note that the signal generator is still sensitive at full actuation, and thus covers the whole range of actuation. Figure 1 has already demonstrated how the deformation of a bellow can be controlled through the bending metric κ.

V. Conclusion and Discussion

We present a method to provide feedback for the deformation control of soft robotic actuators using 3D printed color-patterns. Two designs are presented: 1) an external signal generator that translates a change in strain to a change in color ratio, and 2) an internal signal generator that generates a change in color ratio upon a change in bellow shape.

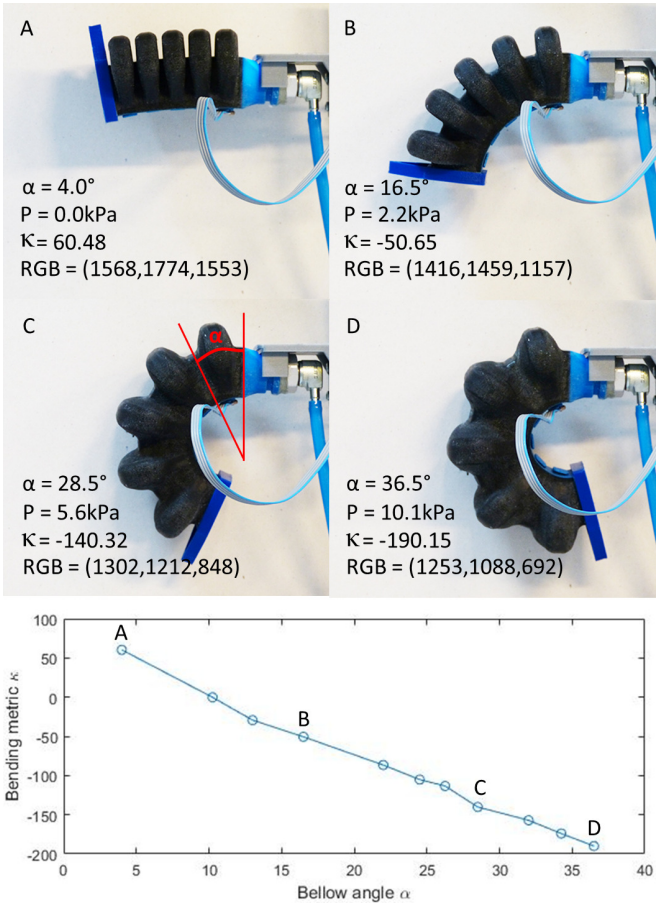

Fig. 12: The bending metric κ plotted w.r.t. the bellow angle α. The angles have been measured over the deformed bellow as indicated at bellow C. The signal is monotonic and sensitive to small changes.

Along with the novel structural design, we have investigated methods for converting the color signals into a monotonic metric that can be used as an indicator for the flexure in bending deformation. The effectiveness of the color-based sensing approach has been verified in experimental tests.

In our current practice (e.g., Fig. 1), the placement of a sensor is determined by trial-and-error to obtain the most sensitive signal. When moving the sensor to the middle of the actuator, the value of κ is less sensitive to the global shape of the actuator. This is because this color-based sensing method only provides information about a local shape deformation. To obtain a precise shape estimation, the data from multiple sensors needs to be fused, which we plan to investigate in the near future. Moreover, different types of deformations, rather than bending, such as twisting and elongation, also will be considered in our future research.

REFERENCES

[1] D. Rus and M. T. Tolley, "Design, fabrication and control of soft robots," *Nature*, vol. 521, 2015.

[2] R. B. N. Scharff, E. L. Doubrovski, W. A. Poelman, P. P. Jonker, C. C. L. Wang, and J. M. P. Geraedts, *Towards Behavior Design of a 3D-Printed Soft Robotic Hand*. Springer International Publishing, 2017, pp. 23–29.

[3] K. C. Galloway, P. Polygerinos, C. J. Walsh, and R. J. Wood, "Mechanically programmable bend radius for fiber-reinforced soft actuators," in *The 16th International Conference on Advanced Robotics (ICAR 2013)*, 2013, pp. 1–6.

[4] R. Deimel and O. Brock, "A novel type of compliant and underactuated robotic hand for dexterous grasping," *International Journal of Robotics Research*, vol. 35, no. 1-3, pp. 161–185, 2016.

[5] A. D. Marchese, K. Komorowski, C. D. Onal, and D. Rus, "Design and control of a soft and continuously deformable 2d robotic manipulation system," in *2014 IEEE International Conference on Robotics and Automation (ICRA)*, May 2014, pp. 2189–2196.

[6] M. Luo, W. Tao, F. Chen, T. K. Khuu, S. Ozel, and C. D. Onal, "Design improvements and dynamic characterization on fluidic elastomer actuators for a soft robotic snake," in *2014 IEEE International Conference on Technologies for Practical Robot Applications (TePRA)*, April 2014, pp. 1–6.

[7] M. D. Grissom, V. Chitrakaran, D. Dienno, M. Csencits, M. Pritts, B. Jones, W. McMahan, D. Dawson, C. Rahn, and I. Walker, "Design and experimental testing of the OctArm soft robot manipulator," in *Unmanned Systems Technology VIII, Proceedings of the SPIE*, vol. 6230, 2006.

[8] J. T. Muth, D. M. Vogt, R. L. Truby, Y. Meng, D. B. Kolesky, R. J. Wood, and J. A. Lewis, "Embedded 3d printing of strain sensors within highly stretchable elastomers," *Advanced Materials*, vol. 26, no. 36, pp. 6307–6312, 2014.

[9] C. Majidi, R. Kramer, and R. J. Wood, "A non-differential elastomer curvature sensor for softer-than-skin electronics," *Smart Materials and Structures*, vol. 20, no. 10, p. 105017, 2011.

[10] C. Lucarotti, M. Totaro, A. Sadeghi, B. Mazzolai, and L. Beccai, "Revealing bending and force in a soft body through a plant root inspired approach," *Scientific Reports*, vol. 5, 2015.

[11] O. Atalay, A. Atalay, J. Gafford, H. Wang, R. Wood, and C. Walsh, "A highly stretchable capacitive-based strain sensor based on metal deposition and laser rastering," *Advanced Materials Technologies*, 1700081.

[12] J. C. Yeo, H. K. Yap, W. Xi, Z. Wang, C.-H. Yeow, and C. T. Lim, "Flexible and stretchable strain sensing actuator for wearable soft robotic applications," *Advanced Materials Technologies*, vol. 1, no. 3, 2016, 1600018.

[13] S. Li, H. Zhao, and R. F. Shepherd, "Flexible and stretchable sensors for fluidic elastomer actuated soft robots," *MRS Bulletin*, vol. 42, no. 2, p. 138142, 2017.

[14] J. Hughes, U. Culha, F. Giardina, F. Guenther, A. Rosendo, and F. Iida, "Soft Manipulators and Grippers: A Review," *Frontiers in Robotics and AI*, vol. 3, no. November, pp. 1–12, 2016.

[15] S. Ozel, E. H. Skorina, M. Luo, W. Tao, F. Chen, Y. Pan, and C. D. Onal, "A composite soft bending actuation module with integrated curvature sensing," in *2016 IEEE International Conference on Robotics and Automation (ICRA)*, May 2016, pp. 4963–4968.

[16] H. Zhao, R. Huang, and R. F. Shepherd, "Curvature control of soft orthotics via low cost solid-state optics," in *2016 IEEE International Conference on Robotics and Automation (ICRA)*, pp. 4008–4013.

[17] H. Zhao, K. OBrien, S. Li, and R. F. Shepherd, "Optoelectronically innervated soft prosthetic hand via stretchable optical waveguides," *Science Robotics*, vol. 1, 2016.

[18] J. Morrow, H. S. Shin, C. Phillips-Grafflin, S. H. Jang, J. Torrey, R. Larkins, S. Dang, Y. L. Park, and D. Berenson, "Improving soft pneumatic actuator fingers through integration of soft sensors, position and force control, and rigid fingernails," in *2016 IEEE International Conference on Robotics and Automation (ICRA)*, May 2016, pp. 5024–5031.

[19] V. Wall, G. Zller, and O. Brock, "A method for sensorizing soft actuators and its application to the rbo hand 2," in *2017 IEEE International Conference on Robotics and Automation (ICRA)*, May 2017, pp. 4965–4970.

[20] P. Polygerinos, Z. Wang, J. T. B. Overvelde, K. C. Galloway, R. J. Wood, K. Bertoldi, and C. J. Walsh, "Modeling of Soft Fiber-Reinforced Bending Actuators," *IEEE Transactions on Robotics*, vol. 31, no. 3, pp. 778–789, 2015.

[21] B. Mosadegh, P. Polygerinos, C. Keplinger, S. Wennstedt, R. F. Shepherd, U. Gupta, J. Shim, K. Bertoldi, C. J. Walsh, and G. M. Whitesides, "Pneumatic Networks for Soft Robotics that Actuate Rapidly," *Advanced Functional Materials*, pp. 2163–2170, 2014.

[22] A. Brunton, C. A. Arikan, and P. Urban, "Pushing the limits of 3d color printing," *ACM Trans. Graphics*, vol. 35, no. 1, pp. 1–13, 2015.